In-Service Buckling of Heated Pipelines

By Roger E. Hobbs[1]

(19)

(Reviewed by the Pipeline Division)

Abstract: Compressive forces may be induced in pipelines by the restraint of axial extensions due to temperature changes or other causes. These forces may cause vertical or lateral buckling of the pipeline. These two buckling modes, which both involve an overall column-type response without gross distortion of the pipeline cross-section, are analyzed on the basis of related work on railroad track. For normal coefficients of friction, the lateral mode occurs at a lower axial load than the vertical mode and is dominant in pipelines unless the line is trenched or buried. The theoretical solutions are illustrated by numerical results for a typical pipeline and some design implications reviewed.

Introduction

The economic importance of submarine pipelines has increased greatly in recent years with the development of offshore oil and gas fields in many parts of the world. The cost in terms of lost production of a failure in such a line is so high that considerable interest has been focused on the stresses caused during the laying (12,16) and modification or repair (5) of submarine pipelines. Similar arguments on a somewhat lower scale of expense apply to pipelines on dry land. However, comparatively little attention has been paid to problems occurring in lines during routine service. This paper addresses one such problem, the assessment of compressive axial forces in the pipeline and their consequences.

The magnitude of the axial load in the pipe depends on many factors. As well as the mechanical properties of the line and its weight coat, the axial force is a function of the initial tension at the seabed just after laying, the pressure difference across the pipe wall and temperature variations due to hot oil passing through the line. These factors interact with seabed geometry and frictional or trench backfill effects, or both, as well as the influence of end restraints in shorter lines: Akten (1) has treated some effects of partial end restraint at a platform tie-in and Yen et al. (17) have described some analogous phenomena in land based pipelines. Finally, the previous loading history and time dependent changes due to scour, currents and tides are also relevant.

Thus it is extremely difficult to say with any certainty what axial force exists at any point in a given pipeline at a given time. Nonetheless, two major causes of compressive forces can be identified, arising from the restraint of the strains associated with thermal and internal pressure loadings. With oil and gas temperatures potentially up to 180° F (100° C) above water temperature and operating pressures over 1,450 lb/in.^{2} (10 N/mm^2) these effects can produce very significant forces indeed in a long line where the necessary frictional force can develop between pipe

[1]Sr. Lecturer, Dept. of Civ. Engrg., Imperial College, London, U.K.

Note.—Discussion open until August 1, 1984. To extend the closing date one month, a written request must be filed with the ASCE Manager of Technical and Professional Publications. The manuscript for this paper was submitted for review and possible publication on January 31, 1983. This paper is part of the *Journal of Transportation Engineering*, Vol. 110, No. 2, March, 1984. ©ASCE, ISSN 0733-947X/84/0002-0175/$01.00. Paper No. 18691.

and seabed, or in shorter lines with effective end restraints. Denoting the cross-sectional area of the pipe by A, Young's Modulus by E, the coefficient of linear thermal expansion by α and the temperature change by T, the force P_o created by full restraint of thermal expansion is, simply,

$$P_o = EA\alpha T \quad \ldots\ldots (1)$$

The free axial strain, ϵ, due to a positive pressure difference p between the oil and the sea is given in terms of the well-known thin wall axial and hoop stresses in the pipe by

$$\epsilon = \frac{1}{E}\left(\frac{pr}{2t} - \nu\frac{pr}{t}\right) \quad \ldots\ldots (2)$$

in which ν is Poisson's ratio, and t and r are the pipe wall thickness and radius respectively. Then, if ϵ is completely restrained, the axial compressive force generated and available to participate in buckling is

$$P_o = EA\epsilon = \frac{Apr}{t}(0.5 - \nu) \quad \ldots\ldots (3)$$

This paper addresses two possible responses to the compressive force generated. Both involve significant bending of the initially straight pipeline, similar to the bending deformation occurring in the elastic (Euler) buckling of an axially loaded column as its critical load is approached. As in a long column fabricated from a circular hollow section, the cross section of the pipe remains circular, at least in the initial stages of buckling, although the responses discussed here may well lead to pipe overstress and local failure by yielding and ovalization. The initial absence of gross cross-sectional distortion may be contrasted with the situation in a propagating buckle triggered by excessive bending and external pressurization during laying operations (13). The first buckling mode (Fig. 1(*a*)) addressed here involves part of the line lifting itself vertically from the seabed, while the second (Fig. 1(*b*)) results in various snaking lateral movements in the horizontal plane against frictional resistance. Both of these modes can be demonstrated in a very simple model employing,

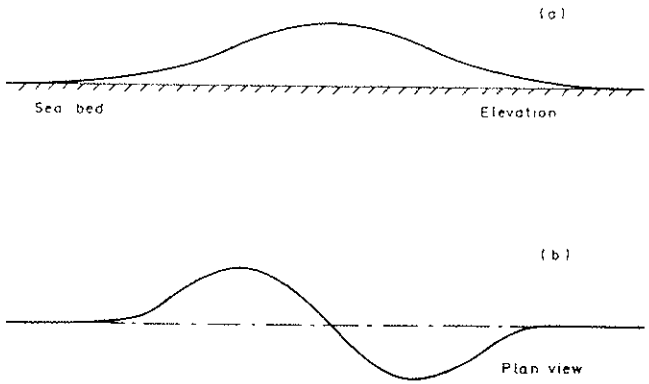

FIG. 1.—Vertical and Lateral Buckling Modes

for example, rubber strips resting on a horizontal machined surface and loaded by a small screw jack, and both have been recorded in pipelines in practice.

Analysis—Vertical Mode

This mode of buckling has attracted a great deal of attention over the years from railway engineers concerned with an analogous problem, the buckling of continuously welded railroad track. Kerr (8) has presented a review paper with nearly 50 references to this problem, while Marek and Daniels (10) have described an apparently independent analysis of the vertical buckling of crane rails. Their work (as corrected in discussion by Granström (3)) agrees in all respects with the theory first developed in 1936 by Martinet (11). Accordingly, it seems appropriate merely to summarize the method and results for the vertical mode at this point. The first step is to solve the linear differential equation for the deflected shape of the buckled part of the pipeline, which is treated as a beam column under uniform lateral load equal to the selfweight. It is assumed that the bending moment at the lift-off point is zero. This assumption has been examined elsewhere (4), and it should also be noted that the use of the linear equation relies on the usual column buckling assumption of small slopes, a point to be borne in mind later when assessing the results. In the notation of Fig. 2(*a*),

$$y'' + n^2 y + \frac{m}{8}(4x^2 - L^2) = 0 \quad \ldots\ldots (4)$$

in which a prime denotes differentiation of the displacement y with respect to the longitudinal coordinate x, the selfweight is w per unit length, and the second moment of area of the pipe is I. $m = w/EI$ and $n^2 = P/EI$, and the buckle length is L. Eq. 4 has the solution

$$y = \frac{m}{n^4}\left(-\frac{\cos nx}{\cos\frac{nL}{2}} - \frac{n^2x^2}{2} + \frac{n^2L^2}{8} + 1\right) \quad \ldots\ldots (5)$$

The unknown length of buckle L is then determined from the condition

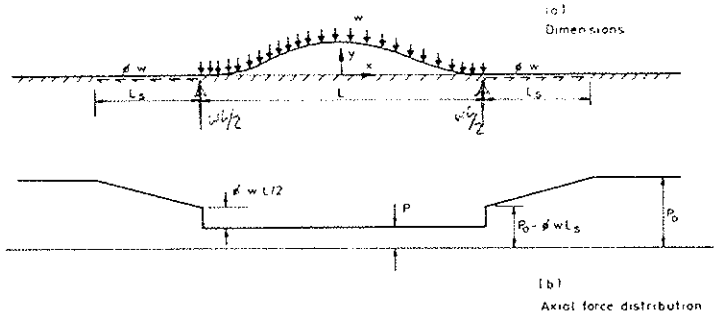

FIG. 2.—Details of Vertical Buckle

that the slope at the ends of the buckle should be zero. This yields

$$\tan\frac{nL}{2} = \frac{nL}{2} \quad \ldots\ldots (6)$$

or as lowest root

$$nL = 8.9868 \ldots\ldots (7)$$

The next step is to compare the axial load P in the buckle with the axial load P_o well away from the buckle (Fig. 2(*b*)). P is clearly less than P_o because of the extra length round the buckle compared to L itself. The drop in force is not as large as would be expected at first glance because two adjacent lengths of pipe L_s slide in towards the buckle—giving the axial force distribution shown in Fig. 2(*b*). The discontinuities in this distribution at each lift-off point are associated with the concentrated vertical reactions of $0.5\,wL$ which occur there.

Setting up a compatibility equation (10), the following results are obtained:

$$P = 80.76\frac{EI}{L^2} \quad \ldots\ldots (8)$$

$$P_o = P + \frac{wL}{EI}[1.597 \times 10^{-5} EA\phi wL^5 - 0.25(\phi EI)^2]^{1/2} \quad \ldots\ldots (9)$$

in which ϕ is the coefficient of friction between pipe and subgrade. The maximum amplitude of the buckle

$$\hat{y} = 2.408 \times 10^{-3}\frac{wL^4}{EI} \quad \ldots\ldots (10)$$

and the maximum bending moment, at $x = 0$, is

$$\hat{M} = 0.06938\,wL^2 \quad \ldots\ldots (11)$$

while the maximum slope is

$$\hat{y}' = 8.657 \times 10^{-3}\frac{wL^3}{EI} \quad \ldots\ldots (12)$$

This last result is useful for checking the validity of the small slope assumption in particular numerical cases, i.e. conventionally $\hat{y}' \leq 0.1$ for "small" slopes. A further result of practical interest is the size of the slipping length adjacent to the buckle,

$$L_s = \frac{P_o - P}{\phi w} - 0.5L \quad \ldots\ldots (13)$$

Thus the minimum theoretical distance between the centers of two adjacent but independent vertical buckles is

$$L + 2L_s = \frac{2(P_o - P)}{\phi w} \quad \ldots\ldots (14)$$

Eq. 9 is awkward and may be compared with the result for a very

large coefficient of friction (i.e., $L_s = 0$)

$$P_o = 80.76\frac{EI}{L^2} + 1.597 \times 10^{-5}\frac{w^2AEL^6}{(EI)^2} \quad \ldots\ldots (15)$$

It is easy to show that Eq. 15 has a minimum at a buckle length

$$\bar{L} = \left[\frac{1.6856 \times 10^6 (EI)^3}{w^2AE}\right]^{0.125} \quad \ldots\ldots (16)$$

Eqs. 15 and 16 are useful when solving Eq. 9 for particular cases as described later.

Analysis—Lateral Modes

The lateral modes observed in a small scale experiment (e.g. Fig. 1(*b*)) all resemble sine curves decaying either side of a central peak amplitude. As a first step, a lateral mode of the same shape as the vertical mode was considered, mode 1 in Fig. 3. With the vertical analysis to hand, it was simple to determine the relationship between buckle length L and axial force P_o for a lateral coefficient of friction assumed equal to the friction coefficient for axial movements of the slipping lengths L_s. Unfortunately, for equilibrium this mode requires concentrated lateral forces of $\phi wL/2$ at the ends of the buckle analogous to the concentrated vertical forces at the lift-off points in the vertical mode. On a rigid seabed concentrated vertical forces are possible (and practical cases closely approach the rigid ideal (4)) but it is not possible to generate a truly concentrated *lateral* force by friction. Refs. 8, 9 and 11 which came to hand rather later deal with this point at length, but in the investigation described here the next step was to repeat the analysis using a different assumption which avoids the difficulty.

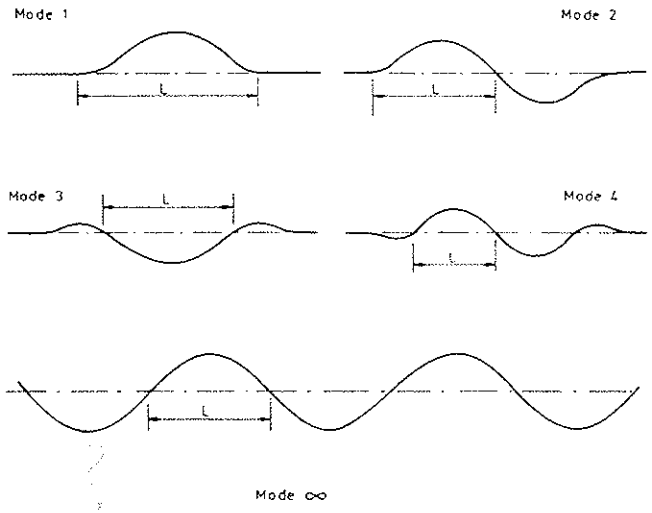

FIG. 3.—Lateral Buckling Modes

Looking at the experimentally observed lateral modes once more, it was assumed that the family of decaying trigonometric curves were all initial imperfection generated variants of one fundamental constant amplitude periodic curve. In other words, it was assumed that an initially perfect pipe would buckle into an indefinite series of half waves as shown in Fig. 3, mode ∞. This assumption has the computational advantages that the nodes of the half wave pattern do not slide parallel to the axis of the pipe and, more importantly, can be made to satisfy lateral equilibrium.

Looking at the consequences of this new assumption in detail, the linear differential equation governing the deflected shape is unchanged, (Eq. 4), except that m is now $\phi w/EI$, i.e., it is assumed that the lateral frictional force is fully mobilized everywhere. The displacement boundary conditions are unchanged but for the zero slope condition at $x = \pm L/2$ which is replaced by a shear force condition at the same location. Thus Eq. 5 still holds with the new value of m, while after careful consideration of signs the shear condition yields the length of the buckle from

$$\tan \frac{nL}{2} = 0 \quad \text{..... (17)}$$

or as the lowest non-trivial root

$$nL = 2\pi \quad \text{..... (18)}$$

Compatibility then requires that

$$P_o - P = \left[\frac{AE}{L}\right] \int_{-L/2}^{L/2} \frac{1}{2} y'^2 \, dx \quad \text{..... (19)}$$

that is: the reduction in axial force in the buckle equals the product of the axial stiffness and the extension round the curve. This leads to the following results for the infinite lateral buckling mode

$$P = 4\pi^2 \frac{EI}{L^2} \quad \text{..... (20)}$$

$$P_o = P + 4.7050 \times 10^{-5} AE \left(\frac{\phi w}{EI}\right)^2 L^6 \quad \text{..... (21)}$$

For computational use, it is noted that this equation has a minimum at

$$\bar{L} = \left[\frac{2.7969 \times 10^5 (EI)^3}{(\phi w)^2 AE}\right]^{0.125} \quad \text{..... (22)}$$

The maximum amplitude of the buckle

$$\hat{y} = 4.4495 \times 10^{-3} \frac{\phi w}{EI} L^4 \quad \text{..... (23)}$$

and the maximum bending moment, at $x = 0$, is

$$\hat{M} = 0.05066 \, \phi w L^2 \quad \text{..... (24)}$$

while the maximum slope is

$$\hat{y}' = 0.01267 \frac{\phi L^3}{EI} \quad \text{..... (25)}$$

Again, if $\hat{y}' \leq 0.1$ in a particular case, the small slope linear differential equation is probably sufficiently accurate.

Refs. 8, 9 and 11 were obtained after completing this analysis. Martinet (11), as long ago as 1936, considered lateral mode 1 as well as the vertical mode, observed the lack of lateral equilibrium at the ends of the buckle and predicted that mode 3 (with a smaller lack of equilibrium at its ends) was likely to develop as a result (Fig. 3). He then analyzed this higher mode, confirming that buckling would be initiated at a lower axial force for a given out-of-straightness than necessary for mode 1. Kerr (8) [and in a condensed form (9)] confirmed Martinet's work for modes 1 and 3 using a variational formulation and presented results for two antisymmetric modes, modes 2 and 4 (Fig. 3). These are initiated at very similar axial force/initial imperfection combinations which are rather smaller than those needed to trigger mode 3. Martinet and Kerr's results are discussed later, but it is worth summarizing their formulas for modes 1–4 (and an extension of their work giving the maximum bending moment) in the notation of the present paper at this point.

Taking the half wavelength of the most significant part of the buckle as L in each case (Fig. 3), and using the constants of Table 1, the reduced axial force within the buckle is given by

$$P = k_1 \frac{EI}{L^2} \quad \text{..... (26)}$$

$$\text{Then} \quad P_o = P + k_3 \, \phi w L \left[\left(1.0 + k_2 \frac{AE \, \phi w L^5}{(EI)^2}\right)^{1/2} - 1.0\right] \quad \text{..... (27)}$$

The maximum amplitude of the buckle relative to the original axis is

$$\hat{y} = k_4 \frac{\phi w}{EI} L^4 \quad \text{..... (28)}$$

while the maximum bending moment $\hat{M}$ is

$$\hat{M} = k_5 \, \phi w L^2 \quad \text{..... (29)}$$

TABLE 1.—Constants for Lateral Buckling Modes

Mode (1)	Constants				
	k_1 (Eq. 26) (2)	k_2 (Eq. 27) (3)	k_3 (Eq. 27) (4)	k_4 (Eq. 28) (5)	k_5 (Eq. 29) (6)
1	80.76	6.391×10^{-5}	0.5	2.407×10^{-3}	0.06938
2	$4\pi^2$	1.743×10^{-4}	1.0	5.532×10^{-3}	0.1088
3	34.06	1.668×10^{-4}	1.294	1.032×10^{-2}	0.1434
4	28.20	2.144×10^{-4}	1.608	1.047×10^{-2}	0.1483
∞	$4\pi^2$	4.7050×10^{-5} (Eq. 21)		4.4495×10^{-3}	0.05066

RESULTS

Figs. 4–6 summarize the results of vertical and lateral mode calculations for a typical pipeline for a variety of coefficients of friction, including the practical range $0.3 \leq \phi \leq 0.7$. The pipe considered has an outside diameter of 25.6 in. (650 mm), and a wall thickness of 0.59 in. (15 mm) giving a cross-sectional area of 46.38 in.^{2} (299.2 cm^2) and a second moment of area 3,625 in.^{4} (150,900 cm^4). Its submerged weight (including concrete coating) has been taken as 260 lb/ft (3.8 kN/m). The results have been presented in terms of the temperature rise necessary to generate the axial force in equilibrium with the buckle lengths and amplitudes shown, and the coefficient of linear thermal expansion, α, has been taken as 11×10^{-6}/°C for this purpose.

The results were obtained from a small computer program using the following procedure which recognizes that it is much easier to find the

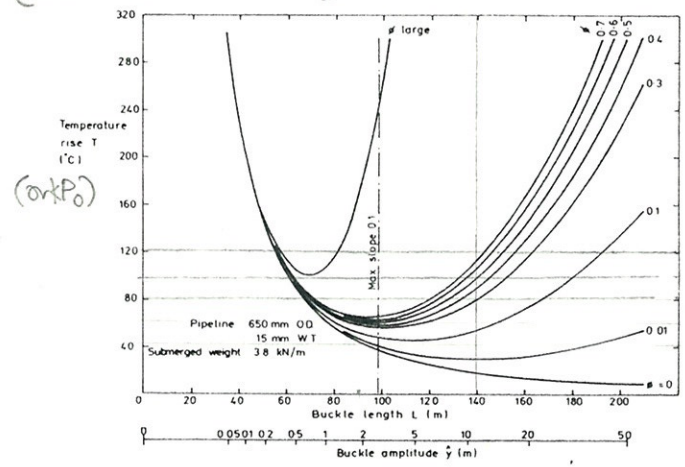

FIG. 4.—Results for Vertical Buckling

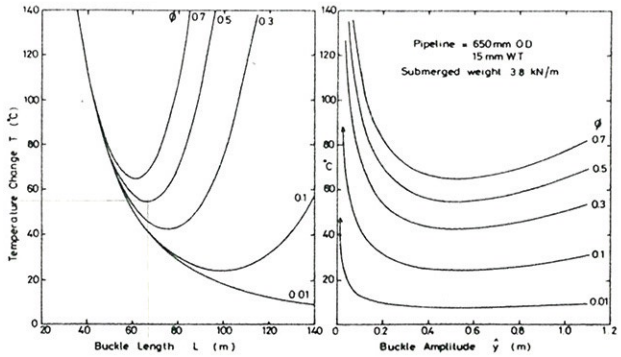

FIG. 5.—Results for Lateral Buckling—∞ Mode

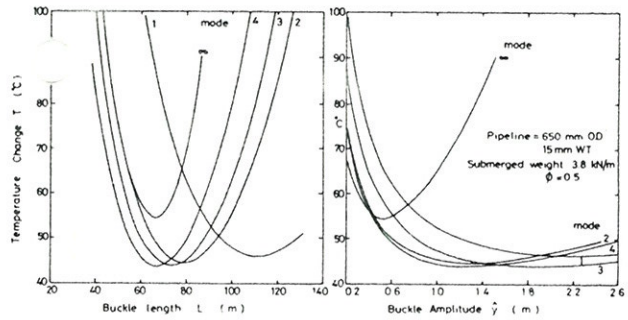

FIG. 6.—Comparison of the Lateral Buckling Modes

force (or temperature change) corresponding to a given buckle length L than vice versa.

1. Vertical mode—high friction coefficient
   (a) Compute $\bar{L}$ using Eq. 16.
   (b) For a range of 20 values of L between 0.1 $\bar{L}$ and 3 $\bar{L}$, compute P_o using Eq. 15, T using Eq. 1, and the buckle amplitude $\hat{y}$ using Eq. 10.
2. Vertical mode—real friction coefficients
   For a range of friction coefficients ϕ, and 20 values of L between $0.1\bar{L}$ and $3\bar{L}$, compute P_o using Eq. 9, T using Eq. 1 and the buckle amplitude $\hat{y}$ using Eq. 10.
3. Lateral modes—infinite mode
   (a) For each of a range of friction coefficients ϕ, compute $\bar{L}$ using Eq. 22.
   (b) For each friction coefficient ϕ, and a range of 20 values of L between $0.5\bar{L}$ and $1.5\bar{L}$, compute P_o using Eq. 21, T using Eq. 1 and the buckle amplitude $\hat{y}$ using Eq. 23.
4. Lateral modes—modes 1–4
   Repeat steps 3a and b using Eqs. 27 and 28 for P_o and $\hat{y}$. To establish the minimum for mode 1 values of L up to $2.0\bar{L}$ may have to be used.

NUMERICAL EXAMPLE

If, as an illustration, the coefficient of friction ϕ is taken as 0.5, Fig. 4 shows that the largest "safe" temperature change to avoid vertical buckling in this particular pipeline is about 61° C. For lateral buckling (Fig. 6) the "safe" temperature change is rather lower, about 44° C. Then, if (as an example) a temperature change between these two figures of say, 45° C is expected, the consequences of later buckling should be checked, while vertical buckling is unlikely to be a problem.

From Fig. 6, buckles in modes 2, 3 and 4 are possibilities at 45° C. From an interpolation of the data used to plot Fig. 6, the half wavelengths of the buckles in these modes are shown in Table 2. Given the wavelength, the amplitude, bending moment and axial force (and hence

TABLE 2.—Numerical Example—Lateral Buckling

Buckling mode (1)	Buckle length L ft (m) (2)	Amplitude $\hat{y}$ ft (m) (3)	Moment $\hat{M}$ 10^3 lb-ft (kN-m) (4)	Axial force P 10^3 lb (kN) (5)	nding plus axial stress 10^3 lb/in.^{2} (N/mm^2) (6)	% of yield if σ_y = 65,000 lb/in.^{2} (448 N/mm^2) (7)
2	268.6 (81.86)	4.96 (1.51)	1,022 (1,386)	413.7 (1,840)	52.1 (359)	80
3	260.3 (79.35)	8.17 (2.49)	1,266 (1,716)	379.7 (1,689)	61.6 (425)	95
4	237.4 (72.36)	5.73 (1.75)	1,088 (1,475)	378.1 (1,682)	54.1 (373)	83

the corresponding bending, axial, and total stresses) can be calculated using Eqs. 28, 29 and 26 respectively. The results of these calculations are included in Table 2, which compares the total stress with the yield point of an API X65 grade line. Mode 3 is clearly the most critical at some 95% of yield. It is concluded that large amplitude buckles are likely to occur, and that large bending stresses will be generated. Thus it would be prudent to reduce the design temperature change or to prevent lateral buckling by raising the effective friction coefficient, perhaps by trenching the line.

Analysis

It is apparent from Figs. 4–6 that the lateral modes become possible at a smaller temperature change than the vertical mode for realistic friction coefficients. Thus unless lateral restraint is provided, by trenching the line for example, the lateral modes will be dominant. This feature is confirmed by small scale experiments and practical experience. An unburied line will snake laterally, while a buried line may burst out of the seabed (or desert!). Once a buried line has lifted, an interaction with the lateral mode may occur, as the buckle itself now has no lateral restraint ($\phi = 0$). Alternatively the buckle may roll or twist laterally.

Figs. 4 and 5 are otherwise very similar and it is useful to discuss the common features in terms of idealized load or temperature against length of buckle and amplitude curves (Fig. 7). The first point is that in theory an ideal, perfectly straight pipeline would not buckle. The pipe is in equilibrium for all values of axial load in an undeformed configuration and while the curve for the deformed shape (Eqs. 9, 15 or 21) approaches the vertical axis asymptotically at high temperatures and small wavelengths, it never quite meets the axis. As Kerr (9) has remarked, this is a consequence of the assumption of fully mobilized friction even for vanishingly small displacements, and the situation may be contrasted with the conventional pin-ended Euler column where the post-buckling equilibrium path actually *crosses* the initial equilibrium path on the axis.

Supposing, next, something marginally less than initial perfection in the pipeline, it is clear that at some temperature T the imperfection will be enough to bridge the gap between the two equilibrium paths, bringing it to the equilibrium position A. The part of the secondary equilibrium path from A to B is clearly unstable, and a dynamic snap will occur

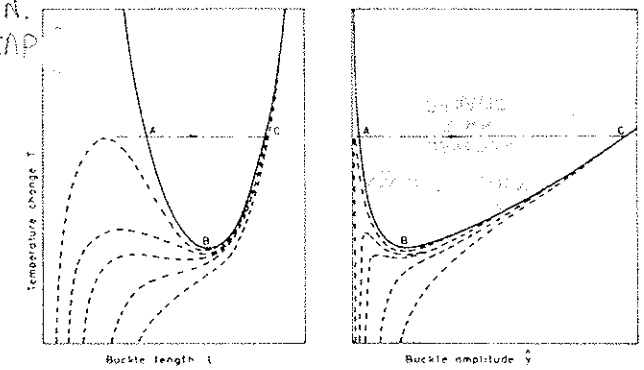

FIG. 7.—Equilibrium Paths and Imperfection Sensitivity-Schematic

from A to C (chain dotted line) at a constant load P_o in the pipeline well away from the buckle, although the buckle itself lengthens and partially unloads. Because, on this argument, no snap can occur below the temperature $\bar{T}$ at B, $\bar{T}$ has been called the "safe" temperature in the railroad literature.

These ideas can be presented with slightly more rigor by considering the temperature/buckle length curves for initially imperfect systems sketched in Fig. 7 (dashed lines). For very small imperfections a large snap is indeed seen experimentally. As the initial out-of-straightness is increased the snap occurs at lower forces and less dramatically. Eventually, for large enough imperfections the snap is eliminated, to be replaced by a single-valued magnification of the initial bow. For any initial imperfection, the behavior is ultimately asymptotic to the stable curve BC for the perfect system.

The behavior indicated in Fig. 7 is supported by recent work by Tvergaard and Needleman (15) on the lateral buckling of initially imperfect railroad tracks. In a finite element analysis in which the buckle wavelength is constrained to be the same as the wavelength of the initial imperfection, and a limited length of track is considered so that unloading into the buckle is restricted, curves similar to Fig. 7 are presented for various initial imperfections, and the most critical initial wavelength identified. It is, however, questionable whether constraining the wavelength to match that of the initial imperfection is completely legitimate, and Kerr (9) has shown that there are significant track length effects. In small scale models substantial wavelength changes do occur during buckling, and the writer feels that more work on the effects of initial imperfection is needed. It is clear that such work will be based on numerical rather than analytical studies. Whether finite element or finite difference (2) studies are used, the buckled wavelength should be free to develop as it will, and parametric studies used to determine the worst-case initial imperfection pattern. Such a study could usefully be complemented by small scale experimental work, using for example a long oil filled 0.5 in. (12.7 mm) copper pipe with an internal heating element.

In practical terms, it may even be desirable to deliberately create initial

out-of-straightness, to eliminate the possibility of a snap. This is simple enough for land based lines which often include dog [illegible] and expansion loops, but it is not so easy for submarine lines. Working from a lay barge, the pipe lengths are welded together with a 1:480 straightness tolerance and sent over the stinger. Deliberate kinks could overstress the line during laying. As the weather worsens involuntary large radius curves may be induced at the seabed by laybarge motion but it is not practical to lay the line to specified radii. Nor is it worth trying; Martinet (11) and small scale experiments both show that a large radius is ineffective in eliminating the snap or in changing its wavelength.

On unloading the pipeline differences appear between the vertical and horizontal modes. A vertical buckle will trace the secondary path back down to B, and, if the load is further reduced, drop back to the straight configuration, although a small residual compression will arise at the site of the buckle because of frictional effects. A chain of horizontal buckles will initially try to trace the path down to B, but the changes in wavelength coupled with the reversal of the lateral friction force will leave it at zero temperature with some residual out-of-straightness and a small tension in the line. On reloading the pipeline these imperfections must predispose the line to buckle laterally at a lower load than before by magnification of the imperfections. In the vertical mode, with small residual axial forces the line is likely to buckle at the same location as before but not necessarily at a significantly reduced temperature as the straightness of the pipe is unimpaired.

As might have been predicted, it is clear from Figs. 4 and 5 that the value of the friction coefficient ϕ only becomes particularly relevant to the results in the post-buckling regime. However, these results do not show any extreme sensitivity to the value of ϕ. Since the value of ϕ for a given stretch of seabed is only known approximately and is not necessarily independent of the magnitude of the displacement this is just as well.

Turning now to a comparison of the various lateral modes, Fig. 6 presents results for the five possibilities considered here for a single friction value, $\phi = 0.5$. It is clear, as Kerr (5) has shown for rail tracks, that the anti-symmetric modes 2 and 4 occur at very similar temperature/initial imperfection combinations, which are rather smaller than those needed to trigger the symmetric mode 3. However, as found in the numerical example presented earlier, mode 3 seems to be associated with rather larger amplitudes and bending stresses. Which of these three modes develops in a particular case is thought to be determined by the initial imperfections in a given pipeline, and with lines over 100 miles (160 km) long now commonplace it is clear that examples of all three modes might be found in a given pipeline. Mode 1, occurring at higher temperatures, seems unlikely to be of practical concern. Mode ∞ is of academic interest because it can be involved in the initiation of the other modes. Referring to Fig. 6, at small amplitudes mode ∞ occurs at lower temperatures than the other modes, but is clearly in unstable equilibrium and will rapidly snap into a large amplitude stable form of one of the other modes. This argument supports the intuitive view of the lateral modes being imperfection generated variants of the ∞ mode. Indeed, Tvergaard and Needleman (15) argue that this process is but one of many examples of

the *localization* of buckling phenomena.

A cautionary [illegible]nt should be made about the analyses of modes 3 and 4, in particular. [illegible]is recognized (8) that they contain an approximation which will lead to an over estimate of the amplitude. In the analyses it has been assumed that the axial force P is constant throughout the entire buckle, in spite of the inward movement from the adjacent unbuckled pipeline. On the contrary, the axial force in the inner half waves of modes 3 and 4 must be significantly less than in the outer, smaller amplitude, half waves because of axial friction and the true amplitude of the inner waves will be smaller as a result. If these arguments were to be extended to modes with 5, 6, 7 ... half waves a situation would rapidly be reached where the inner, most significant, buckles were not receiving any energy at all from the inward sliding of the unbuckled line, and indeed the inner waves would approach the conditions assumed in the analysis of mode ∞. This, then, is a cogent argument for not pursuing the present analysis route (with constant axial force) to modes higher than 4 half waves, because it is unrealistic. On the other hand, a more realistic calculation is most unlikely to produce lower "safe" temperatures than modes 2, 3 and 4 because mode ∞ has a higher "safe" temperature than these modes. The analyses of modes 2, 3 and 4 presented here can therefore be recommended for lower bound design use.

Finally, the following limitations of the analyses presented in this paper should be borne in mind:

1. Only perfect systems have been rigorously examined. In the vertical mode no account has been taken of the initial out-of-straightness, and the approach to the lateral mode needs further numerical or experimental development or both. The classical column (Fourier) analysis of initial lack of straightness is inappropriate here because the buckled length changes progressively as the load increases. It is some comfort to know that the magnitude and nature of the initial imperfections in pipelines as laid are also unknown, and extremely difficult to assess, so that an improved analysis would not of itself be very helpful except as a lower bound design aid.
2. Perfect elasticity and small slopes have been assumed. The analyses presented assume that the full elastic modulus of the pipe is available to resist bending. Once plasticity occurs the analysis loses its validity: yielding will obviously leave its mark on the pipe on unloading and act as an imperfection on subsequent reloading. Of course, most linepipe is competent to develop a plastic hinge without effect on its serviceability.

The analyses also use the linear differential equation for bending which is strictly true only for small slopes, conventionally less than 0.1 radian. However, more exact elliptic integral solutions have been obtained for cantilevers (14) and pin-ended columns (6). In the cantilever, for an axial load 1.5% greater than that predicted by the linear equation, the end slope is 0.35 radians. Similarly, in the pin-ended column, for an axial load 1.2% greater than the Euler load, the greatest slope is 0.31 radians. These results suggest that the 0.1 radian limit on "small" slopes is rather conservative; a cut-off line corresponding to this limit has been marked on Fig. 4 as a guide, and true loads beyond this limit may be rather higher than shown. The 0.1 radian limit is not exceeded in Fig. 5.

Conclusions

Two potential buckling mechanisms in pipelines subjected to axial compression have been identified and analyzed. It is found that horizontal snaking modes occur at a lower axial load than the vertical mode, and a horizontal mode is therefore dominant unless lateral restraint is provided by trenching when an interactive buckling mode becomes possible. Full account has been taken of friction between the pipe and the ground in the vertical mode, relying on two independent but formally identical references on the buckling of rail tracks and crane rails. An analysis of a lateral mode involving an infinite sequence of half waves with fully developed lateral friction has been presented and compared with earlier work on isolated buckles over a shorter length which involve longitudinal as well as lateral sliding.

The effects of imperfections, unloading and reloading are discussed and it is concluded that further numerical work on the effects of initial imperfections would be valuable. The theoretical solutions are illustrated by numerical results for a typical pipeline.

Acknowledgment

The author is indebted to Dr. Taylor and Mr. Gan (Sheffield Polytechnic) for pointing out significant corrections to the numerical values in Eqs. 21 and 22.

Appendix I.—References

1. Akten, H. T., "New Developments in Submarine Pipeline In-Place Stability Analysis," *Proceedings of Arctic/Offshore/Deepsea Systems Symposium*, American Society of Mechanical Engineers, New Orleans, 1982.
2. Cassell, A. C., and Hobbs, R. E., "Numerical Stability of Dynamic Relaxation Analysis of Non-linear Structures," *International Journal of Numerical Methods in Engineering*, Vol. 10, 1976, pp. 1407–1410.
3. Granström, A., discussion of "Behavior of Continuous Crane Rails" by P. S. Marek and J. H. Daniels, *Journal of the Structural Division*, ASCE, Vol. 98, No. ST1, Jan., 1972, pp. 360–361.
4. Hobbs, R. E., "The Effect of Soil Modulus on Pipeline Stresses," *Journal of the Transportation Engineering Division*, ASCE, Vol. 106, No. TE6, Nov., 1980, pp. 775–786.
5. Hobbs, R. E., "Solutions for Pipeline Tie-in and Repair Problems," *Proceedings Second Symposium on Offshore Mechanics and Arctic Engineering*, American Society of Mechanical Engineers, Houston, Tex., 1983, pp. 538–552.
6. Horne, M. R., and Merchant, W., *The Stability of Frames*, Pergamon, Oxford, 1965, pp. 10–12.
7. Kerr, A. D., "On the Stability of the Railroad Track in the Vertical Plane," *Rail International*, Vol. 5, Feb., 1974, pp. 132–142.
8. Kerr, A. D., "Analysis of Thermal Track Buckling in the Lateral Plane," *Acta Mechanica*, Vol. 30, 1978, pp. 17–50.
9. Kerr, A. D., "On Thermal Buckling of Straight Railroad Tracks and the Effect of Track Length on the Track Response," *Rail International*, Vol. 9, Sept. 1979, pp. 759–768.
10. Marek, P. J., and Daniels, J. H., "Behavior of Continuous Crane Rails," *Journal of the Structural Division*, ASCE, Vol. 97, No. ST4, Apr., 1971, pp. 1081–1095.
11. Martinet, A., "Flambement des Voies sans Joints sur Ballast et Rails de Grand Longueur" ("Buckling of Tracks without Joints on Ballast and Very Long Rails" in French), *Revue Générale des Chemins de Fer*, Vol. 55/2, 1936, pp. 212–230.
12. Palmer, A. C., Hutchinson, G., and Ells, J. W., "Configuration of Submarine Pipelines during Laying Operations," *Transactions of ASME, Journal of Engineering for Industry*, Vol. 96, 1974, pp. 1112–1118.
13. Palmer, A. C., and Martin, J. H., "Buckle Propagation in Submarine Pipelines," *Nature*, Vol. 254, Mar., 1975, pp. 46–48.
14. Timoshenko, S. P., and Gere, J. M., *Theory of Elastic Stability*, 2nd ed., McGraw-Hill, Kogakusha, New York, 1961, pp. 76–81.
15. Tvergaard, V., and Needleman, A., "On Localized Thermal Track Buckling," *International Journal of Mechanical Sciences*, Vol. 23, No. 10, 1981, pp. 577–587.
16. Wilhoit, J. C., Jr., and Merwin, J. E., "Pipe Stresses Induced in Laying Offshore Pipelines," *Transactions of ASME, Journal of Engineering for Industry*, Vol. 89, 1967, pp. 37–43.
17. Yen, B. C., Tsao, C. H., and Hinkle, R. D., "Soil-Pipe Interaction of Heated Oil Pipelines," *Journal of the Pipeline Division*, ASCE, Vol. 107, No. TE1, Jan., 1981, pp. 1–14.

Appendix II.—Notation

The following symbols are used in this paper:

A = cross-sectional area;
E = Young's modulus;
I = second moment of area of cross section;
$k_1k_2k_3k_4k_5$ = constants—see Table 1;
L = length of buckle;
L_s = length of slipping pipe adjacent to buckle;
M = bending moment;
m = w/EI;
n = $(P/EI)^{1/2}$;
P = axial force in buckled pipe;
P_o = prebuckling axial force;
p = pressure;
r = radius;
T = temperature increment;
t = wall thickness of pipe;
w = submerged weight of pipeline (including weight coat) per unit length;
x = coordintate along pipe axis;
y = coordinate perpendicular to pipe axis;
α = coefficient of linear thermal expansion;
ϵ = strain;
ϕ = coefficient of friction;
ν = Poisson's ratio; and
σ_y = yield stress.

Superscripts

$\hat{}$ = peak, maximum value;
$'$ = first derivative, slope;
$''$ = second derivative, curvature; and
$\bar{}$ = value associated with the "safe" temperature increment.